Biophys J BioFAST, published on May 30, 2008 as doi:10.1529/biophysj.108.133173

The hydrophobic insertion mechanism of membrane curvature generation by proteins

Felix Campelo[1,2], Harvey T. McMahon[3], Michael M. Kozlov[1]
[1]Department of Physiology and Pharmacology, Sackler Faculty of Medicine, Tel Aviv University, 69978 Tel Aviv, Israel

[2] Departament d'Estructura i Constituents de la Matèria, Facultat de Física, Universitat de Barcelona Diagonal 647, E-08028, Barcelona, Spain

[3]MRC Laboratory of Molecular Biology, Hills Road, Cambridge, CB2 0QH, UK

Corresponding author:
Michael M. Kozlov,
Department of Physiology and Pharmacology,
Sackler Faculty of Medicine,
Tel Aviv University,
69978 Tel Aviv, Israel
Phone: +972-3-6407863
Fax: +972-3-6409113
E-mail: michk@post.tau.ac.il

Running title: Membrane bending by hydrophobic insertions

Key words: membrane curvature, amphipathic helix, N-BAR domains, vesicle budding, membrane elasticity, membrane trafficking

Abstract
A wide spectrum of intracellular processes is dependent on the ability of cells to dynamically regulate membrane shape. Membrane bending by proteins is necessary for the generation of intracellular transport carriers and for the maintenance of otherwise intrinsically unstable regions of high membrane curvature in cell organelles. Understanding the mechanisms by which proteins curve membranes is therefore of primary importance. Here we suggest for the first time a quantitative mechanism of lipid membrane bending by hydrophobic or amphipathic rod-like inclusions which simulate amphipathic α-helices– structures shown to sculpt membranes. Considering the lipid monolayer matrix as an anisotropic elastic material, we compute the intra-membrane stresses and strains generated by the embedded inclusions, determine the resulting membrane shapes and the accumulated elastic energy. We characterize the ability of an inclusion to bend membranes by an effective spontaneous curvature, and show that shallow rod-like inclusions are more effective in membrane shaping than are lipids having a high propensity for curvature. Our computations provide experimentally testable predictions on the protein amounts needed to generate intracellular membrane shapes for various insertion depths and membrane thicknesses. We also predict that the ability of N-BAR domains to produce membrane tubules *in vivo* can be ascribed solely to insertion of their amphipathic helices.

Introduction

Most cellular membranes have regions of very high curvature yet lipid bilayers resist bending (1). Therefore, active production of membrane curvature is one of the major challenges faced by a cell in the course of formation of its internal organelles and generation of membrane transport containers. How proteins can produce and stabilize the enormous range of membrane curvatures that exist *in vivo* is beginning to be understood.

Generation of high membrane curvature requires action of specialized membrane associated proteins (2-4). These can either function as direct effectors by interactions with the membrane or as indirect scaffolds interacting with membranes via linking proteins (3). The list of proteins and protein complexes shown to be crucial for strong bending of membranes is constantly expanding (5-22). Complexes of clathrin with accessory proteins (2, 23), and COPI and COPII coat-complexes (7, 24, 25) generate small vesicles. Narrow membrane tubules are produced by proteins of the dynamin family (see e.g. (19, 26-29)), BAR domain-containing proteins (9, 10, 12, 13, 15, 18, 22), epsins (11), EHD-family proteins (8), C2 domain-containing proteins, such as synaptotagmins (17), and proteins of the reticulon and DP1/Yop1 families (20, 21).

Quantitative elaboration of the physical mechanisms by which proteins bend membranes is indispensable for classification of the rapidly accumulating phenomenology on the effects of proteins on membrane curvature and the understanding of the relationships between the structure of a protein and its efficiency in membrane shaping. It was suggested that proteins can generate the membrane curvature either by embedding small hydrophobic or amphipathic regions into the membrane matrix (see for reviews (3, 4)) or by attaching the membrane surface to the intrinsically curved protein scaffolds by virtue of cognate charge interactions (3, 30).

A common realization of the former mode of membrane bending referred to as the hydrophobic insertion mechanism is through a shallow embedding of amphipathic helices into the upper part of a lipid monolayer. Epsins were the first proteins shown to induce membrane curvature by amphipathic helix insertion (11). On interaction with phosphatidylinositol-4,5-biphosphate polar groups amphipathic α-helices fold and embed into the lipid monolayer matrix, transforming the flat membrane into tubules of ~20 nm diameter (11). Small G-proteins Arf1 and Sar1 expose amphipathic α-helices upon exchange of GDP to GTP, which results in the anchoring of such proteins to lipid bilayers and the subsequent bilayer bending (6, 14, 16). Amphipathic helices of N-BAR domains of amphiphysin and endophilin bind peripherally in the bilayer resulting in the midpoint of the helix insertion being aligned with the phosphate level of the lipid headgroups. This insertion is essential for generation of membrane tubules of 35-50 nm diameter which get converted into vesicles of the same diameter at increased amounts of the protein (13, 18). The C2A and C2B domains of synaptotagmin-1 interact in Ca^{2+}-dependent manner with the polar groups of negatively charged phospholipids and insert hydrophobic loops into the lipid monolayers at a depth of up to third of the monolayer thickness (31) resulting in the formation of narrow membrane tubes of ~17 nm diameter (17).

A number of proteins have the potential to scaffold membranes into curved shapes. These include dynamin family proteins (26, 32), BAR superfamily proteins (3, 12, 15), EHD2 (8), the clathrin coat (33) and COPI/IIcoats (25). Notably, scaffolding proteins can contain hydrophobic and/or amphipathic fragments able to penetrate the membrane to a certain depth, thus contributing to the membrane

curvature generation. For example, while dynamin forms a helical oligomer capable of scaffolding high curvature, the variable loops of its PH domain are suggested to interact with the membrane and the VL1 loop is proposed to insert into the membrane (34-37). The efficiency of membrane bending by N-BAR domains depends crucially on the integrity of their amphipathic helices (3, 13). COPI, COPII, and some clathrin adaptors, are recruited to the membrane by small G-proteins (Arf1p for AP1 and COPI, and Sar1p for COPII), which couple their respective scaffolding apparatuses to the potential to bend membranes by insertion of the amphipathic α-helices (38). The reticulons and DP1/Yop1 family proteins possess two long hydrophobic hairpin segments which could induce membrane curvature changes by forming a wedge that occupies more space in the upper than the lower leaflet of a lipid bilayer (21).

Hence, it is becoming clear that the majority of membrane bending proteins may employ membrane insertion of hydrophobic or amphipathic regions with, in some cases, a coupling to scaffolding domains.

Here, for the first time we suggest and analyze quantitatively a mechanism by which the amphipathic and hydrophobic insertions bend membranes into tubular shapes with diameters of a few tens of nanometers. The analysis is based on a physical model of lipid monolayers. Our computations show that membrane insertions like amphipathic α-helices are more powerful in membrane bending than use of "non-bilayer" lipids, and that biologically relevant numbers of such insertions are sufficient to create even the extreme membrane curvatures of intracellular organelles and transport intermediates. Our analysis also considers the role of lipid monolayer coupling in curvature generation and demonstrates that shallow insertions are best suited to the production of high membrane curvature. We draw the experimentally testable predictions on the dependence of the membrane curvature on the bilayer thickness and the membrane area fraction occupied by the amphipathic helices.

Qualitative essence of membrane bending by hydrophobic inclusions

We consider an initially flat lipid membrane with rod-like inclusions inserted into its interior (Fig. 1). To grasp the major features of the mechanism of membrane bending by inclusions, we address here a simple case of two-dimensional deformations, meaning that the membrane adopts a form of a tube with rod-like inclusions ordered in rows along the tubular axis. The membrane shape is then characterized by the form of the tube cross-section. The diameter of the inclusion rod is assumed to be 1 nm, which is typical for an amphipathic α-helix with side chains; the lipid monolayer thickness is taken to be 2 nm.

The inclusion pushes aside the elements of the membrane matrix and produces, in this way, the intra-membrane strains and stresses leading to the accumulation of elastic energy. The curving of the membrane from the initial flat configuration results in the partial relaxation of these stresses and minimizes the elastic energy.

While being a part of a peripheral membrane protein, an amphipathic α-helix has a shallow membrane matrix penetration possibility. However, for generality and a broader understanding of the physics of membrane bending by small inclusions, we consider the effects of different modes of insertion including those where the inclusions reach the bilayer mid plane. The cases of deep insertions can account for membrane bending by isolated hydrophobic inclusions such as synthetic peptides mimicking fusion peptides.

An inclusion inserted into one membrane monolayer results in curving of the whole bilayer. The extent of the bilayer bending depends on the way the monolayers

are coupled to each other. There are two kinds of such coupling (Fig.2). Due to their mutual attachment along the common hydrophobic interface the monolayers are always coupled in the transverse direction (perpendicular to the membrane plane). In addition, there may be monolayer coupling in the in-plane direction meaning that the areas of the two monolayers can not change independently (39).

In most of the biologically relevant circumstances the inclusions are inserted only into small fragments of a large membrane such as the membrane regions destined for conversion into intracellular membrane carriers (Fig. 2a). The two monolayers of such a fragment can, independently of each other, exchange their areas with the rest of the membrane, the latter providing a large reservoir of lipids (Fig. 2a). Due to the free and independent exchange of lipid between the reservoir and each of the monolayers of the membrane fragment in question, there is no in-plane coupling between the latter. The in-plane coupling comes into play if the inclusions are inserted across the whole area of a closed membrane. This happens, for example, in *in vitro* experiments where proteins are added to liposomes and embed without spatial restriction everywhere across the entire surfaces of the lipid membranes (Fig. 2b). In this case, there is no reservoir for the monolayer area exchange, and, provided that the effects of slow flip-flop of lipid molecules between the monolayers can be neglected, the expansion of one monolayer cannot proceed independently of deformation of the second monolayer.

Membrane monolayers subject to the transverse coupling only, will be referred to as the *laterally uncoupled* monolayers. In cases where there exists also in-plane coupling, the monolayers will be called *laterally coupled*. While *in vitro* experiments on liposome membrane curvature may not therefore closely mimic the *in vivo* situation, the potential for lateral monolayer coupling at the plasma membrane exists and may be provided by, for example, actin based corrals, which would limit lipid exchange with endocytic sites. For completeness we model both possibilities.

Consider first the case of *laterally coupled* monolayers. A shallow insertion of inclusions into the upper monolayer expands its upper part, while the rest of this monolayer underneath the inclusions and the lower monolayer resist this expansion. To minimize the generatedT stresses that are asymmetrically distributed through the bilayer depth, the membrane must bulge towards the upper monolayer (Fig. 3a). According to a common convention, curvature resulting from bulging in this direction is defined as positive. A somewhat deeper insertion up to the middle of the upper monolayer expands this monolayer (Fig. 3b). Because of the lateral coupling between the monolayers, this expansion is opposed by the lower monolayer. According to the monolayer area asymmetry model (39), this leads to further generation of asymmetric stresses within the membrane and a positive membrane curvature (Fig. 3b). If the inclusion penetrates deeper into the membrane and reaches its mid plane, the strains and stresses are distributed symmetrically within the bilayer (Fig. 3c), so that bending in either direction will not relax the elastic energy. Such insertion does not induce membrane bending but results in the overall expansion of the membrane area (Fig. 3c). An even deeper inclusion insertion expands the lower membrane part with respect to its upper part, which results in bending towards the lower monolayer and, hence, generation of a negative curvature (Fig. 3d).

In the case of *laterally uncoupled* monolayers with inclusion inserted in the upper leaflet of the membrane, a qualitative consideration similar to the above one has to be applied to the upper monolayer only. Due to the transverse coupling between the monolayers, bending of the upper monolayer will result in bending also of the lower one, and, hence, of the whole membrane. Therefore, similarly to the above case of

coupled monolayers, shallow insertions generating asymmetric strains in the upper monolayer produce a positive curvature of the latter and of the whole membrane (Fig.4a). However, a bare expansion of the upper monolayer by an inclusion reaching its middle (Fig. 4b) will not result in the membrane bending since the upper monolayer can expand independently of the lower one due to the lipid exchange with the reservoir. As a result, for this depth of the inclusion insertion the membrane will be flat (Fig. 4b). This is different from the above case of coupled monolayers, in which insertion up to the middle of the upper monolayer resulted in the membrane curvature (Fig.3b). Penetration of an inclusion into the lower part of the upper monolayer generates its negative curvature, and, hence, a negative curvature of the whole membrane (Fig.4c).

Model

Elastic model of a lipid monolayer. A large literature exists on modeling membrane deformations by proteins spanning the whole lipid bilayer and generating small membrane curvatures (40-44). These studies employ the Helfrich model of bending elasticity considering a membrane as an elastic surface (1). Here we can not use this common description since the cross-section of an inclusion in question is smaller than the lipid monolayer thickness and we are interested in the intra-membrane deformations for different depths of the inclusion insertion generating large curvatures. Therefore, we consider a lipid monolayer as a three-dimensional layer with finite thickness and bulk elastic properties. To describe the system, we use the standard theory of elasticity of an anisotropic three-dimensional medium (45). The volume density of the elastic energy is determined by

$$f = \sigma_{ik}^{0} u_{ik} + \frac{1}{2}\lambda_{iklm} u_{ik} u_{lm}, \qquad (1)$$

where σ_{ik}^{0} is the tensor of the initial intra-monolayer stresses existing before the inclusion insertion, λ_{iklm} is the tensor of the elastic moduli of the monolayer interior, and u_{ik} is the strain tensor related to the displacement vector u_l of the monolayer elements by $u_{ik} = \frac{1}{2}\left(\frac{\partial u_i}{\partial \xi^k} + \frac{\partial u_k}{\partial \xi^i}\right)$, ξ^j being the coordinates (45).

Since we consider only the tubule-like shapes of membranes, we choose the Cartesian system of coordinates, with the *x*-*y*-axes lying in the initial membrane plane, the *y*-axis directed along the tube axis, and *x*-axis lying in the tube cross-section originating ($x = 0$) in the middle of inclusion (Fig. 1). The *z*-axis points towards the hydrophilic heads and originates (*z*=0) at the bottom surface of the monolayer. The position of the inclusion will be characterized by the coordinate of its center, z_{inc}.

As the lipid material has properties of an isotropic liquid in the lateral (x-y) direction and of a solid film in the transverse *z*-direction, the system is described by only four independent elastic moduli (Appendix A): the moduli of volume stretching-compression in the lateral, $\lambda_{xxxx} = \lambda_{yyyy}$, and normal, λ_{zzzz}, directions; the modulus of coupling between these two kinds of deformation, λ_{xxzz}; and the modulus of transverse shear deformation, λ_{xzxz}.

For a quantitative analysis we need the values of all these bulk elastic moduli and their dependencies on the position within the lipid monolayer matrix.
To the best of our knowledge, only little experimental information has been obtained on the local elastic moduli of the lipid monolayer matrix. The orientational and

positional average of the volume compressibility of lipid material was measured to constitute about $5 \cdot 10^{-11} \frac{cm^2}{dyne}$ (46) meaning that the corresponding averaged volume stretching-compression elastic modulus is $2 \cdot 10^9 \frac{N}{m^2}$. Yet separate measurements exist neither of anyone of the four bulk elastic moduli, nor of their dependence on the position within the monolayer. At the same time, the values have been determined for the overall elastic moduli characterizing a lipid monolayer as a surface, namely, the moduli of monolayer bending, $\kappa \approx 4 \cdot 10^{-20} J$ (47), area stretching-compression, $\Gamma \approx 0.1 N/m$ (48), and tilt of the lipid hydrophobic chains with respect to the membrane plane, $\kappa_t \approx 0.03 N/m$ (49, 50). In addition, experimental studies revealed position within lipid monolayers of the so called neutral surface, an intra-monolayer plane for which the deformations of bending and stretching-compression are energetically decoupled (51-53). For monolayers of different lipid compositions, the neutral surface was found to lie close to the interface between the lipid polar heads and the hydrocarbon tails at a depth of about one third of the monolayer thickness, meaning that the coordinate of neutral surface can be taken to be $z_N = \frac{2}{3} h$.

There are few relationships between the bulk elastic moduli of the monolayer material and the overall elastic moduli of lipid monolayer as a surface. The transverse shear modulus λ_{xzxz} can be related to the monolayer tilt modulus κ_t by

$$\int_0^h \lambda_{xzxz} dz = \kappa_t \,, \qquad (2)$$

where the integration is performed over the monolayer thickness h. We will assume that the two volume stretching-compression moduli are equal at any position within the monolayer, $\lambda_{xxxx} = \lambda_{zzzz}$, and denote their values by λ_{ST}. The modulus λ_{ST} and the coupling modulus λ_{xxzz} are related to the overall monolayer stretching-compression modulus Γ by

$$\int_0^h \lambda_{ST} \left(1 - \frac{\lambda_{xxzz}^2}{\lambda_{ST}^2}\right) dz = \Gamma \,. \qquad (3)$$

Finally, the position of the monolayer neutral surface (51-53), z_N, corresponds to vanishing first moment of $\lambda_{ST}\left(1 - \frac{\lambda_{xxzz}^2}{\lambda_{ST}^2}\right)$,

$$\int_0^h \lambda_{ST} \left(1 - \frac{\lambda_{xxzz}^2}{\lambda_{ST}^2}\right)(z - z_N) dz = 0 \qquad (4)$$

The bulk elastic moduli must satisfy the relationships Eqs.(2-4).

To satisfy Eq.4 for the position of the neutral surface z_N, we assume that the moduli λ_{ST} and λ_{xxzz} have different values in the regions of the lipid polar heads and the hydrocarbon tails. Taking the interface between these two regions to lie at $z_0 = \frac{2}{3} h$, we present the two bulk moduli as step functions

$$\lambda_{ST} = \begin{cases} \lambda_{ST}^{h}, & z_0 < z < h \\ \lambda_{ST}^{t}, & 0 < z < z_0 \end{cases} \text{ and } \lambda_{xxzz} = \begin{cases} \lambda_{xxzz}^{h}, & z_0 < z < h \\ \lambda_{xxzz}^{t}, & 0 < z < z_0 \end{cases}. \qquad (5)$$

Inserting Eq.5 into Eq.4 and requiring that, in accord with the measurements, the coordinate of the neutral surface coincides with that of the interface between the polar groups and the hydrocarbon tails, $z_N = z_0 = \frac{2}{3}h$, we obtain $\lambda_{ST}^{t}(1 - \frac{\lambda_{xxzz}^{t2}}{\lambda_{ST}^{t2}}) = \frac{1}{4}\lambda_{ST}^{h}(1 - \frac{\lambda_{xxzz}^{h2}}{\lambda_{ST}^{h2}})$. Taking into account this relationship together with Eq.3 and a requirement that the positional average of the bulk stretching-compression modulus is $\frac{1}{h}\int_0^h \lambda_{ST} dz = 2 \cdot 10^9 \frac{N}{m^2}$, we obtain $\lambda_{ST}^{h} = 4 \cdot 10^9 N/m^2$, $\lambda_{xxzz}^{h} = 3.93 \cdot 10^9 N/m^2$, $\lambda_{ST}^{t} = 10^9 N/m^2$, $\lambda_{xxzz}^{t} = 0.98 \cdot 10^9 N/m^2$.

The transverse shear modulus is assumed to be constant through the monolayer thickness and equal $\lambda_{xzxz} = 1.5 \cdot 10^7 N/m^2$.

In the case of coupled monolayers, we take a vanishing shear modulus λ_{xzxz} at the interface between the two monolayers.

We assume the inclusions to be much more rigid than the lipid material, and, therefore, neglect the potential for the inclusions themselves to be deformed.

Computations. The equilibrium membrane configurations can be found by solving a set of equations for the intra-monolayer displacements u_l following from minimization of the elastic energy (Eq.1) (45). We assume that the inclusions are evenly distributed along the circumference of the membrane tube cross-section, and using the related symmetry of the cross-section shape we perform calculations for a membrane element corresponding to half distance between the neighboring inclusions (Fig. 1). The total membrane shape is composed of such elements.

The equilibrium equations along with the boundary conditions and the details of the computation procedure are presented in the Appendix B.

To analyze the case of the laterally uncoupled monolayers, we compute the deformations of an isolated monolayer and determine the effective monolayer curvature J_S^m generated by the inclusions (Appendix B). The curvature of the bilayer mid plane, J_S^b, can then be expressedT, with good accuracy, through the induced curvatures of the upper, J_S^{out}, and lower, J_S^{in}, monolayers, $J_S^b = \frac{1}{2} \cdot (J_S^{out} - J_S^{in})$.

In the case of laterally coupled monolayers, we compute deformations of the bilayer as a whole, accounting for the ability of the monolayers to locally slide with respect to each other, in spite of the global coupling between their areas, by taking a vanishing shear modulus λ_{xzxz} at the interface between the two monolayers.

To analyze the results, it is convenient to relate the induced curvature to the area fraction occupied by the inclusions on the membrane surface,

$$\phi = \frac{r}{L}, \qquad (6)$$

where r is the radius of the inclusion cross-section and L is the half distance between the inclusions (Fig. 1).

In the case of an isolated monolayer, we present this relation in the form

$$J_S^m = \varsigma_{inc} \cdot \phi , \qquad (7)$$

where J_S^m is the monolayer curvature and ς_{inc} can be seen as a spontaneous curvature of an effective particle composed of the inclusion and the deformed portion of the lipid matrix. The value ς_{inc} referred to below as the inclusion spontaneous curvature can, in general, depend on the area fraction ϕ.

In the case of laterally coupled monolayers, where the computed value is the curvature of the bilayer, J_S^b, we will use the relationship

$$J_S^b = \frac{1}{2}\varsigma_{inc} \cdot \phi , \qquad (8)$$

taking into account that the tendency of one monolayer to bend due to the inclusion insertion is offset by the second monolayer and the resulting bilayer curvature is smaller than the favored monolayer curvature by a factor of two.

T We perform here the calculations for a vanishing initial intra-monolayer stress profile, $\sigma_L^0(x)$. Analysis presented in the Appendix C shows that $\sigma_L^0(x)$, does not significantly change the induced membrane curvature.

We perform the calculations by the designated COMSOL Multiphysics 3.3 software.

Results

Isolated monolayer (laterally uncoupled monolayers). A typical conformation of a bilayer consisting of laterally uncoupled monolayers with inclusions inserted at a relatively large distance from each other is presented in Fig.5. The internal strains and stresses of the lipid matrix are maximal near the inclusion and decay along the monolayer with a characteristic length ξ of a few nanometers. Such an order of magnitude of the relaxation length could be expected based on the ratio between the overall shear, $\kappa_t = 30$ mN/m, and bending, $\kappa = 4 \cdot 10^{-20}$ J, moduli of a lipid monolayer $\sqrt{\frac{\kappa}{\kappa_t}} \approx 1nm$ (49).

The monolayer as a whole undergoes sharp bending within the strained areas around the inclusions and remains nearly flat in the regions between the inclusions where the strains vanish. The resulting monolayer shape is not smoothly circular but can be characterized by an effective curvature J_s^m (see Appendix B). Dependence of J_s^m on the inclusion area fraction ϕ (Eq.6) is presented in Fig.6 for a depth of insertion typical for amphipathic α-helices (13). This dependence appears linear unless ϕ approaches the values for which the distance between the adjacent inclusions is comparable to the decay length of the intra-monolayer stresses, ξ. For even smaller inter-inclusion distances, the growth of J_s^m with increasing ϕ becomes stronger than linear (Fig.6).

In the range of the linear dependence of J_s^m on ϕ, the effective spontaneous curvature of the inclusion, ς_{inc}, defined according to Eq.7, is constant and represents a convenient characteristic of the capability of the inclusion to curve the monolayer. The value of the inclusion spontaneous curvature is presented in Fig.7a as a function

of the insertion depth. In early stages of insertion ς_{inc} grows with the insertion depth and reaches its maximal value when more than half of the inclusion cross-section is embedded into the monolayer matrix. The maximal value of ς_{inc} corresponds to the insertion depth of about 40% of the monolayer thickness ($0.4 \cdot h$) typical for the amphipathic α-helices (13). Further insertion of the inclusion results in the monolayer unbending and the inclusion spontaneous curvature vanishes when the center of the inclusion attains a position just above the monolayer mid plane. Continuation of the inclusion insertion results in generation of a negative monolayer curvature (Fig. 7a).

It is instructive to determine the dependence of the effective inclusion spontaneous curvature ς_{inc} on the lipid monolayer thickness, h, which is variable for different cell membranes. This dependence is illustrated in Fig. 8. The value of ς_{inc} is weakly dependent on h (Fig.8(a)). The slow decrease of ς_{inc} with increasing h is illustrated in Fig.8(b) for the insertion depth of about 0.8nm characteristic for the amphipathic α-helices.

Laterally coupled monolayers. A representative conformation of a bilayer with laterally coupled monolayers containing inclusions is presented in Fig.5c. The spontaneous curvature of the inclusion, ς_{inc}, determined according to Eq.8 from the computed bilayer curvature J_S^b is presented in Fig.7b. There is a qualitative difference between the behavior of ς_{inc} in the cases of laterally uncoupled and coupled monolayers. In the latter case ς_{inc} remains positive for all depths of the inclusion penetration into the upper membrane monolayer, while in the former case ς_{inc} changes its sign as discussed above. The reason for this difference is stretching of the upper monolayer area induced by the inclusions, which has no effect on the curvature for the case of laterally uncoupled monolayers but generates a positive contribution to the bilayer curvature in the case of laterally coupled monolayers. At the same time, in the cases of both laterally uncoupled and coupled monolayers, the inclusion spontaneous curvature reaches its maximum for shallow insertions of the inclusion into the membrane matrix (Fig.7).

We define the energetic penalty of the inclusion insertion as the elastic energy accumulated within the monolayer matrix in the course of embedding of the inclusion. The density of this energy per unit length of the cylindrical inclusion is presented in (Fig.9) as a function of the insertion depth. The non-monotonous character of this function is related to the uneven profile of the intra-monolayer elastic moduli (Eq.3) and a complex distribution of strains generated within the monolayer matrix by a cylindrical inclusion. For the typical depth of $0.4 \cdot h$, the energy density is $1.2 k_B T$/nm.

The hydrophobic insertion mechanism is sufficient for N-BAR domains to tubulate membranes. The N-BAR domains constitute one of best explored groups of protein modules capable of membrane bending *in vivo* and *in vitro* (9, 10, 13, 18). The N-BAR domain-containing proteins amphiphysin and endophilin are very important for membrane budding in endocytosis, and their N-BAR domains were shown to convert flat lipid bilayers into tubules of 35 to 50 nm diameter (13, 18). As mentioned in the introduction, the N-BAR domains have the potential to bend membranes according to two mechanisms: scaffolding the membrane by attaching its surface to the crescent-shaped BAR dimer, and by inserting amphipathic helices into the

membrane matrix. Dimerization of N-BAR domains results in an effective local concentration of the amphipathic helices underneath the BAR scaffold, and, hence, enhances the ability of the protein to bend membranes. A question arises about the contribution of the hydrophobic insertion mechanism to the membrane tube formation by N-BAR domains and whether this mechanism may solely drive the entire membrane bending process.

To answer this question we computed the area fraction ϕ of the α-helices needed to produce membrane tubes of 35 to 50 nm diameter. The results are illustrated in Fig.10, which presents the range of the required values of ϕ for different depths of insertion of the α-helices. We found that for a broad range of insertion depths, the required inclusion area fractions ϕ are fewer than 15%. For the most relevant depths of around $0.4 \cdot h$, to produce the experimentally observed curvature, only 7-10% of the tubule area has to be occupied by the inclusions in the case of laterally uncoupled monolayers and 9-15% for laterally coupled monolayers. The obtained values of ϕ are feasible. Indeed, according to crystallographic measurements the total area occupied in the membrane plane by one N-BAR dimer and one α-helix are about ~47 nm^2 and ~6 nm^2, respectively. Hence, for amphiphysin, which has two α-helices per N-BAR dimer, the maximal possible area fraction ϕ corresponding to a complete coverage of the membrane by the N-BAR domains is about 25%. For endophilin having four α-helices per N-BAR dimer assuming that the second amphipathic helix on each N-BAR monomer has the same length and inserts to the same depth, the maximal ϕ can approach 50%. In both cases, the limit of the α-helix area fraction is considerably larger than the inclusion amount required to induce the 35-50 nm tubes. This means that the hydrophobic insertion mechanism alone may drive the experimentally observed membrane bending by N-BAR domains. However, given that BAR domain alone can generate membrane curvature in vitro, one should not ignore the significance of this structure. Given the potency of curvature generation by amphipathic helix insertions it is likely that BAR domains function more as curvature stabilizers/limiters (or sensors).

Discussion

We computed the membrane deformations generated by cylindrical inclusions which model the amphipathic α-helices inserted into the membrane matrix, and analyzed the dependence of the resulting membrane curvature on the depth of the inclusion insertion and the area fraction occupied by the inclusions on the membrane surface. We considered the effects of inclusions in two cases. In the first case, perhaps most relevant for the intracellular processes of membrane bending, the membrane monolayers are laterally uncoupled. This corresponds to a situation where the inclusions are inserted only into a small fragment of a large membrane for example representing the site of a forming endocytic vesicle on the plasma membrane. In the second case, which is likely most relevant for *in vitro* experiments with lipid vesicles (or areas of intracellular membranes where lateral translocation of lipids is limited), the inclusions are inserted along the whole membrane and the membrane monolayers are laterally coupled.

Amphipathic helices are potent membrane curvature generators. According to Fig. 6, the dependence of the induced monolayer curvature, J_S^m, on the inclusion surface fractions ϕ is practically linear as long as the inclusions do not occupy more

than 10% of the membrane surface ($\phi < 0.1$) which corresponds to inter-inclusion separations that are larger than 10nm. Under these conditions, the effective spontaneous curvature of the inclusion, ς_{inc}, determined according to Eq.7, is a convenient characteristic of the ability of the inclusion to bend lipid monolayers. A representative value of ς_{inc} corresponds to a typical penetration depth of the amphipathic helices, which constitutes about 40% of the monolayer thickness (13) ($z_{inc} = 1.7$nm, in Fig. 7). According to Fig.7, such a penetration depth provides the maximal possible value of the inclusion spontaneous curvature which, in the case of laterally uncoupled monolayers, equals $\varsigma_{inc} \approx 0.75\text{nm}^{-1}$. It is instructive to compare this value with the spontaneous curvatures of phospholipids.

While the inclusion spontaneous curvature is positive i.e. produces membrane bulging towards the polar heads, most phospholipids have a negative spontaneous curvature (4). The exceptions are lysolipids which lack one out of two hydrocarbon chains and phospholipids whose polar heads carry an electric charge such as phosphatidylserine and phosphatidic acid under neutral pH. The largest positive spontaneous curvature of physiologically relevant lipids measured to date is that of lysophosphatidylcholine (LPC) and equals $\varsigma_{LPC} \approx 0.26nm^{-1}$ (54). LPC belongs to the class of so-called "non-bilayer" lipids since they do not self-organize in bilayer structures in the absence of canonical lipids necessary for bilayer integrity. Hence, according to our computations, the inclusion spontaneous curvatureT ς_{inc} is considerably larger than the spontaneous curvatures measured for any of the positively curved non-bilayer lipids. This means that amphipathic α-helices are more powerful than phospholipids in generating positive membrane curvature.

Repartitioning of non-bilayer lipids does not impede membrane bending by inclusions. It may be argued that bending of cell membranes containing lipids of different kinds by amphipathic inclusions will be much weaker than that predicted by the present study which assumes a homogeneous lipid composition. Indeed cell membranes include a small fraction of non-bilayer lipids such as diacylglycerol (DAG) which are characterized by strongly conical effective molecular shapes or a large negative spontaneous curvature (53). Redistribution of such lipid molecules into the direct proximity of the inclusions may considerably reduce the stresses generated by the inclusions, and hence, weaken the membrane tendency to bend. Estimations based on our results show however, that this effect is unlikely to be significant. Indeed, a maximal elastic energy, which can be released by one conically shaped lipid molecule approaching the helical inclusion, can be estimated as $\mu_{relax} = -l_{lip} \cdot f_{el}$, where $l_{lip} \approx 0.8$ nm is the lipid dimension in the membrane plane and f_{el} is the accumulated elastic energy per unit length of the inclusion. Based on Fig. 9, for the typical insertion depth of the amphipathic α-helices ($z_{inc} \approx 1.7$nm) the value of f_{el} in the biologically relevant case of laterally uncoupled monolayers is $f_{el} \approx 1.2k_BT/nm$, meaning that $\mu_{relax} \approx -1k_BT$. At the same time, the entropic penalty for the lipid redistribution can be estimated as $\mu_{ent} = -k_BT \cdot \ln c_{lip}$ per lipid molecule, where c_{lip} is the molar fraction of the strongly conically shaped lipid in the membrane and $\kappa_BT \approx 0.6$ kcal/mol is the product of the Boltzmann constant and the absolute temperature. Taking into account that the molar fraction of molecules such as DAG in

cell membranes is small and can be estimated as $c_{lip} \le 0.001$, the entropic penalty is $\mu_{ent} \ge 7k_BT$, which exceeds the energy gain by an order of magnitude, $|\mu_{ent}| >> |\mu_{relax}|$. Hence, the redistribution effects must be minor.

Sensitivity of results to the model's assumptions and parameters. The major assumption of our model is a step-like profile of distribution through the lipid monolayer matrix of the local elastic moduli (Eq.5). To test the sensitivity of the model predictions to this assumption, we repeated the calculations for a completely different trans-monolayer distribution of the elastic moduli, which also satisfies the experimental data. We assumed a homogeneous distribution of the elastic moduli λ_{ST} and λ_{xxzz} throughout the whole monolayer thickness except for the plane $z = \frac{2}{3}h$, where the elastic moduli were larger than elsewhere (a δ-function like profile). The results were similar to those presented above (not shown) meaning that the predictions are insensitive to the details of the unknown distribution of the intra-membrane elasticity.

Another issue concerns the specific parameter values we used and which are not known accurately. The major parameter is the transverse shear modulus λ_{xzxz}. We performed computations for several values of this parameter, as well as for different monolayer thicknesses and different inclusion radii, varying within reasonable ranges. The results demonstrate that the sensitivity to these parameters of the effective spontaneous curvature of the inclusion, which is the major output of this study, is weak (Appendix D). While the elastic energy of the inclusion insertion does exhibit a noticeable dependence on the parameter values (Appendix D), it remains of the same order of magnitude so that the qualitative conclusions based on this energy do not change.

We presented the results for inclusions having a shape of a cylindrical rod with a radius corresponding to the size of a typical α-helix with side chains. Probing computation for a square-like cross-section of the inclusions provided very similar values (not shown) of the inclusion effective spontaneous curvature showing that the major predictions of the model are insensitive to the details of the inclusion shapes. The dependence of the results on the size of the inclusion cross-section is presented in the Appendix D (Fig. D4). While the inclusion effective spontaneous curvature does change with the radius of the inclusion cross-section, qualitatively, these changes are not significant.

Finally, the present work addresses two-dimensional deformations of the membrane. Preliminary computations (results not shown) demonstrate that three-dimensional membrane deformations generated by rod-like inclusions mimicking amphipathic α-helices are characterized by curvatures very similar to those obtained in the present study (to be published elsewhere).

Conclusions. Insertion of small hydrophobic inclusions into the upper part of membrane monolayers is a potent method for proteins to induce membrane curvatures *in vivo*. Notably, there are differences in the physics of bending by inclusions for the cases ofT laterally coupled and uncoupled membrane monolayers. In the biologically relevant case of laterally uncoupled monolayers the "shallowness" of the inclusion insertion is crucial for the membrane bending. The "shallow" membrane inclusions penetrating about 40% of monolayer thickness (13) are predicted to be extremely

effective in membrane shaping and their ability to produce positive curvatures considerably exceeds that of non-bilayer lipids.

Appendix A

Non-vanishing components of the tensor of elastic moduli.

The contribution to the elastic energy of an arbitrary anisotropic medium (Eq.1 of the main text) depending on the elastic moduli

$$f = \frac{1}{2}\lambda_{iklm}u_{ik}u_{lm}, \qquad \text{(A1)}$$

can be simplified for the lipid monolayer, which has properties of an isotropic liquid in the lateral (x-y) direction. In this case, the energy (Eq.A1) must be invariant with respect to rotations around the z-direction perpendicular to the x-y plane. Analysis of the system with such symmetry showed (45) that there are only five independent components of the elastic modulus tensor, which are λ_{xxxx} , λ_{zzzz}, λ_{xxzz}, λ_{xzxz}, λ_{xxyy}. The corresponding elastic energy per unit volume is given by (45)

$$\begin{aligned} f = {} & \frac{1}{4}\left(\lambda_{xxxx}+\lambda_{xxyy}\right)\left(u_{xx}+u_{yy}\right)^2+\frac{1}{2}\lambda_{zzzz}\left(u_{zz}\right)^2+\lambda_{xxzz}\left(u_{xx}+u_{yy}\right)u_{zz} \\ & +2\lambda_{xzxz}\left[\left(u_{xz}\right)^2+\left(u_{yz}\right)^2\right]+\frac{1}{4}\left(\lambda_{xxxx}-\lambda_{xxyy}\right)\left[\left(u_{xx}-u_{yy}\right)^2+4\left(u_{xy}\right)^2\right], \end{aligned} \qquad \text{(A2)}$$

the last term of this expression corresponding to the lateral shear. Because of the lateral fluidity of the monolayer, the energy of the lateral shear must vanish meaning that $\lambda_{xxxx}=\lambda_{xxyy}$. The final form of the free energy is

$$f = \frac{1}{2}\lambda_{xxxx}\left(u_{xx}+u_{yy}\right)^2+\frac{1}{2}\lambda_{zzzz}{u_{zz}}^2+\lambda_{xxzz}\left(u_{xx}+u_{yy}\right)u_{zz}+2\lambda_{xzxz}\left({u_{xz}}^2+{u_{yz}}^2\right), \qquad \text{(A3)}$$

and the only four non-vanishing independent elastic moduli are λ_{xxxx} , λ_{zzzz}, λ_{xxzz}, λ_{xzxz} .

Appendix B

Equilibrium equations and their solution.

We derive the equilibrium equations based on the local force balance. The condition of local mechanical equilibrium, which is a vanishing total force acting on each infinitesimal element of the system, is expressed through the gradient of the stress tensor σ_{ik} by (45)

$$\frac{\partial\sigma_{ik}}{\partial\xi_k}=0. \qquad \text{(B1)}$$

The stress tensor, $\sigma_{ik}=\lambda_{iklm}u_{lm}+\sigma_{ik}^0$, consists of a contribution of the deformation expressed by a product of the strain tensor u_{lm} and the elastic modulus tensor λ_{iklm}, and the initial stresses σ_{ik}^0. In the following we will consider only the former contribution to the stress tensor since σ_{ik}^0 must satisfy on its own the equation (Eq.B1) provided that the initial configuration is an equilibrium one.

Based on Eq.B1, we can write one equilibrium equation for each spatial direction. To this end, we first express explicitly the components of the stress tensor through the strains. Using the relationships between the non-vanishing components of

the elastic modulus tensor $\left(\lambda_{xxxx}=\lambda_{yyyy}=\lambda_{xxyy},\lambda_{zzzz},\lambda_{xzxz}=\lambda_{yzyz},\lambda_{xxzz}=\lambda_{yyzz}\right)$ derived in the Appendix A, the components of the stress tensor can be presented as

$$\begin{aligned}
&\sigma_{xx}=\sigma_{yy}=\lambda_{xxxx}\left(u_{xx}+u_{yy}\right)+\lambda_{xxzz}u_{zz},\\
&\sigma_{zz}=\lambda_{zzzz}u_{zz}+\lambda_{xxzz}\left(u_{xx}+u_{yy}\right),\\
&\sigma_{xz}=2\lambda_{xzxz}u_{xz},\\
&\sigma_{yz}=2\lambda_{xzxz}u_{yz}.
\end{aligned} \tag{B2}$$

Plugging these relations into Eq.B1 and after some algebra, we get the equilibrium equations for a monolayer with rotational invariance with respect to the *z*-axis and lateral fluidity

$$\begin{cases}
\lambda_{xxxx}\left(\dfrac{\partial^2 u_x}{\partial x^2}+\dfrac{\partial^2 u_y}{\partial x\partial y}\right)+\lambda_{xzxz}\dfrac{\partial^2 u_x}{\partial z^2}+\left(\lambda_{xxzz}+\lambda_{xzxz}\right)\dfrac{\partial^2 u_z}{\partial x\partial z}=0\\
\lambda_{xxxx}\left(\dfrac{\partial^2 u_y}{\partial y^2}+\dfrac{\partial^2 u_x}{\partial x\partial y}\right)+\lambda_{xzxz}\dfrac{\partial^2 u_y}{\partial z^2}+\left(\lambda_{xxzz}+\lambda_{xzxz}\right)\dfrac{\partial^2 u_z}{\partial y\partial z}=0\\
\lambda_{xzxz}\left(\dfrac{\partial^2 u_z}{\partial x^2}+\dfrac{\partial^2 u_z}{\partial y^2}\right)+\lambda_{zzzz}\dfrac{\partial^2 u_z}{\partial z^2}+\left(\lambda_{xxzz}+\lambda_{xzxz}\right)\left(\dfrac{\partial^2 u_x}{\partial x\partial z}+\dfrac{\partial^2 u_y}{\partial y\partial z}\right)=0
\end{cases}. \tag{B3}$$

Now, considering the case of two-dimensional deformations, where the y-axis represents the tubular axis, we can simplify the former set of equations,

$$\begin{cases}
\lambda_{xxxx}\dfrac{\partial^2 u_x}{\partial x^2}+\lambda_{xzxz}\dfrac{\partial^2 u_x}{\partial z^2}+\left(\lambda_{xxzz}+\lambda_{xzxz}\right)\dfrac{\partial^2 u_z}{\partial x\partial z}=0\\
\lambda_{xzxz}\dfrac{\partial^2 u_z}{\partial x^2}+\lambda_{zzzz}\dfrac{\partial^2 u_z}{\partial z^2}+\left(\lambda_{xxzz}+\lambda_{xzxz}\right)\left(\dfrac{\partial^2 u_x}{\partial x\partial z}\right)=0
\end{cases}. \tag{B4}$$

The equilibrium equations (Eq.B4) have to be solved for a membrane element related to one inclusion as illustrated in Fig.1. To derive the boundary conditions for this solution, we characterize the position of the inclusion by coordinates of its center: $x=0$, and $z=z_{inc}$. Based on the circular shape of the inclusion cross-section, the horizontal displacement u_x at the left boundary of the membrane element, $x=0$, must be:

$$u_x(x=0,z)=\begin{cases}0 & : \quad z<z_{inc}-r\\ \sqrt{r^2-(z-z_{inc})^2} & : \quad z\geq z_{inc}-r\end{cases}, \tag{B5}$$

where r is the inclusion radius.

The vertical displacement at the left boundary must be constant for the region of insertion,

$$u_z(x=0,z)=z_0^{left} \text{ for } z\geq z_{inc}-r. \tag{B6}$$

The top and bottom surfaces of the monolayer elements are free, and, therefore, the stresses σ_{ik} must vanish on these boundaries.

Finally, the right boundary of the membrane element separated from the left one by a distance L, is a symmetry plane. Therefore, it must remain straight but can rotate with respect to the left boundary by certain angle θ and get shifted in the horizontal and vertical directions by x_0^{right} and z_0^{right}, respectively.

We solve numerically the equilibrium equations (Eq. B4) with the above mentioned boundary conditions. We then compute the elastic energy of the obtained conformation by integrating the energy density (Eq.1 of the main text) over the volume of the membrane fragment, and seek for the parameter values z_0^{left}, z_0^{right}, x_0^{right} and θ corresponding to minimum of this energy. The resulting parameters determine the final membrane shape.

Although the obtained membrane shape is not ideally circular (Fig.2) we can define its effective curvature, J_S, by the relationship

$$J_S = \frac{\sin\theta}{L + x_0^{right}}, \qquad \text{(B7)}$$

where the values of θ and $L + x_0^{right}$ are found in the course of the energy minimization.

Appendix C

Effect of the initial lateral stress profile

To model the distribution of the initial stresses over the monolayer thickness, we follow the results of the extensive previous studies of this issue (55) and assume the initial stresses to be directed only along the monolayer plane and to be isotropic in this plane $\sigma_{xx}^0 = \sigma_{yy}^0 = \sigma_L^0(z)$. We take the distribution of $\sigma_L^0(z)$ through the monolayer thickness to be similar to the stress profile found by computer simulations (56). The parameters of this distribution, have to be specified based on the relationship between $\sigma_L^0(z)$ and the monolayer spontaneous curvature in the initial state J_s^0 determined at the neutral surface,

$$J_S^0 = -\int_0^h \sigma_L^0(z)\cdot(z - z_N)dz \Big/ \int_0^h 2\lambda_{ST}\left(1 - \frac{\lambda_{xxzz}^2}{\lambda_{ST}^2}\right)\cdot(z - z_N)^2 dz, \qquad \text{(C1)}$$

where the integration is performed over the monolayer thickness. The initial stress profile we use corresponds to the monolayer spontaneous curvature of $J_S^0 = -0.1\,\text{nm}^{-1}$ characterizing the most abundant lipid DOPC (57).

We took into account the initial inter-monolayer stress profile, $\sigma_L^0(z)$, by computing deformation of the whole bilayer in the case of laterally coupled monolayers. According to our results, $\sigma_L^0(x)$, practically, does not change the bilayer conformation and, consequently, the inclusion spontaneous curvature (Fig. C1). This is expected since the effects of a non-vanishing $\sigma_L^0(z)$ on the shapes of the two monolayers mutually compensate and do not affect the bilayer shape. At the same time, the energetic penalty of the inclusion insertion is sensitive to $\sigma_L^0(z)$. Fig.C2 represents the elastic energy density per unit length on the cylindrical inclusion for the case of laterally coupled monolayers with and without $\sigma_L^0(z)$. According to these results, the initial stress profile noticeably alters the energetic penalty of the inclusion insertion.

Appendix D

Sensitivity of the results to the value of the system parameters.

We explored the sensitivity of the computed membrane curvature induced by the inclusions and the energy penalty of the inclusion insertion to the value of the monolayer transverse shear modulus which is not known with a good accuracy and of the lipid bilayer thickness which varies for different cell membranes.

Fig. D1 shows that the inclusion spontaneous curvature ς_{inc} is practically independent of the specific value of λ_{xzxz} as long as the latter remains within a reasonable range.

Figs. D2 and D3 illustrate the sensitivity of the results obtained for the case of coupled monolayers to the monolayer thickness h and the transverse shear modulus λ_{xzxz}. Dependence of ς_{inc} of the parameters is similar to that obtained for the uncoupled monolayers. The energy penalty is weakly sensitive to the values of h but varies considerably with λ_{xzxz}.

Fig. D4 shows the dependence of the effective spontaneous curvature of the inclusion on the inclusion radius for both laterally uncoupled (Fig. D4a) and coupled (Fig. D4b) monolayers. The sensitivity of these results to the inclusion radius is weak for a reasonable range of the inclusion size.

Acknowledgements
We are grateful to Leonid Chernomordik and Gary Doherty for helpful discussions. Financial support for MMK by the Israel Science Foundation (ISF) and the Marie Curie Network "Flippases" is gratefully acknowledged.

References

1. Helfrich, W. 1973. Elastic Properties of Lipid Bilayers: Theory and Possible Experiments. Z. Naturforsch. 28c:693-703.
2. Kirchhausen, T. 2000. Three ways to make a vesicle. Nat Rev Mol Cell Biol 1:187-198.
3. McMahon, H. T., and J. L. Gallop. 2005. Membrane curvature and mechanisms of dynamic cell membrane remodelling. Nature 438:590-596.
4. Zimmerberg, J., and M. M. Kozlov. 2006. How proteins produce cellular membrane curvature. Nat Rev Mol Cell Biol 7:9-19.
5. Antonny, B. 2006. Membrane deformation by protein coats. Current opinion in cell biology 18:386-394.
6. Antonny, B., S. Beraud-Dufour, P. Chardin, and M. Chabre. 1997. N-terminal hydrophobic residues of the G-protein ADP-ribosylation factor-1 insert into membrane phospholipids upon GDP to GTP exchange. Biochemistry 36:4675-4684.
7. Bremser, M., W. Nickel, M. Schweikert, M. Ravazzola, M. Amherdt, C. A. Hughes, T. H. Sollner, J. E. Rothman, and F. T. Wieland. 1999. Coupling of coat assembly and vesicle budding to packaging of putative cargo receptors. Cell 96:495-506.
8. Daumke, O., R. Lundmark, Y. Vallis, S. Martens, P. J. Butler, and H. T. McMahon. 2007. Architectural and mechanistic insights into an EHD ATPase involved in membrane remodelling. Nature 449:923-927.
9. Farsad, K., and P. De Camilli. 2003. Mechanisms of membrane deformation. Current opinion in cell biology 15:372-381.
10. Farsad, K., N. Ringstad, K. Takei, S. R. Floyd, K. Rose, and P. De Camilli. 2001. Generation of high curvature membranes mediated by direct endophilin bilayer interactions. The Journal of cell biology 155:193-200.
11. Ford, M. G., I. G. Mills, B. J. Peter, Y. Vallis, G. J. Praefcke, P. R. Evans, and H. T. McMahon. 2002. Curvature of clathrin-coated pits driven by epsin. Nature 419:361-366.
12. Frost, A., P. De Camilli, and V. M. Unger. 2007. F-BAR proteins join the BAR family fold. Structure 15:751-753.
13. Gallop, J. L., C. C. Jao, H. M. Kent, P. J. Butler, P. R. Evans, R. Langen, and H. T. McMahon. 2006. Mechanism of endophilin N-BAR domain-mediated membrane curvature. The EMBO journal 25:2898-2910.
14. Goldberg, J. 1998. Structural basis for activation of ARF GTPase: mechanisms of guanine nucleotide exchange and GTP-myristoyl switching. Cell 95:237-248.
15. Henne, W. M., H. M. Kent, M. G. Ford, B. G. Hegde, O. Daumke, P. J. Butler, R. Mittal, R. Langen, P. R. Evans, and H. T. McMahon. 2007. Structure and analysis of FCHo2 F-BAR domain: a dimerizing and membrane recruitment module that effects membrane curvature. Structure 15:839-852.
16. Lee, M. C., L. Orci, S. Hamamoto, E. Futai, M. Ravazzola, and R. Schekman. 2005. Sar1p N-terminal helix initiates membrane curvature and completes the fission of a COPII vesicle. Cell 122:605-617.
17. Martens, S., M. M. Kozlov, and H. T. McMahon. 2007. How synaptotagmin promotes membrane fusion. Science (New York, N.Y 316:1205-1208.

18. Peter, B. J., H. M. Kent, I. G. Mills, Y. Vallis, P. J. Butler, P. R. Evans, and H. T. McMahon. 2004. BAR domains as sensors of membrane curvature: the amphiphysin BAR structure. Science (New York, N.Y 303:495-499.
19. Praefcke, G. J., and H. T. McMahon. 2004. The dynamin superfamily: universal membrane tubulation and fission molecules? Nat Rev Mol Cell Biol 5:133-147.
20. Shibata, Y., G. K. Voeltz, and T. A. Rapoport. 2006. Rough sheets and smooth tubules. Cell 126:435-439.
21. Voeltz, G. K., W. A. Prinz, Y. Shibata, J. M. Rist, and T. A. Rapoport. 2006. A class of membrane proteins shaping the tubular endoplasmic reticulum. Cell 124:573-586.
22. Frost, A., R. Perera, A. Roux, K. Spasov, O. Destaing, E. H. Egelman, P. De Camilli, and V. M. Unger. 2008. Structural basis of membrane invagination by F-BAR domains. Cell 132:807-817.
23. Schmid, S. L. 1997. Clathrin-coated vesicle formation and protein sorting: an integrated process. Annual review of biochemistry 66:511-548.
24. Kirchhausen, T. 2007. Making COPII coats. Cell 129:1251-1252.
25. Lee, M. C., E. A. Miller, J. Goldberg, L. Orci, and R. Schekman. 2004. Bi-directional protein transport between the ER and Golgi. Annual review of cell and developmental biology 20:87-123.
26. McNiven, M. A., H. Cao, K. R. Pitts, and Y. Yoon. 2000. The dynamin family of mechanoenzymes: pinching in new places. Trends Biochem Sci 25:115-120.
27. Roux, A., K. Uyhazi, A. Frost, and P. De Camilli. 2006. GTP-dependent twisting of dynamin implicates constriction and tension in membrane fission. Nature 441:528-531.
28. Sever, S., H. Damke, and S. L. Schmid. 2000. Garrotes, springs, ratchets, and whips: putting dynamin models to the test. Traffic 1:385-392.
29. Hinshaw, J. E. 2000. Dynamin and its role in membrane fission. Annual review of cell and developmental biology 16:483-519.
30. Blood, P. D., and G. A. Voth. 2006. Direct observation of Bin/amphiphysin/Rvs (BAR) domain-induced membrane curvature by means of molecular dynamics simulations. Proceedings of the National Academy of Sciences of the United States of America 103:15068-15072.
31. Herrick, D. Z., S. Sterbling, K. A. Rasch, A. Hinderliter, and D. S. Cafiso. 2006. Position of synaptotagmin I at the membrane interface: cooperative interactions of tandem C2 domains. Biochemistry 45:9668-9674.
32. Song, B. D., and S. L. Schmid. 2003. A molecular motor or a regulator? Dynamin's in a class of its own. Biochemistry 42:1369-1376.
33. Fotin, A., Y. Cheng, P. Sliz, N. Grigorieff, S. C. Harrison, T. Kirchhausen, and T. Walz. 2004. Molecular model for a complete clathrin lattice from electron cryomicroscopy. Nature 432:573-579.
34. Burger, K. N., R. A. Demel, S. L. Schmid, and B. de Kruijff. 2000. Dynamin is membrane-active: lipid insertion is induced by phosphoinositides and phosphatidic acid. Biochemistry 39:12485-12493.
35. Mears, J. A., P. Ray, and J. E. Hinshaw. 2007. A corkscrew model for dynamin constriction. Structure 15:1190-1202.
36. Zhang, P., and J. E. Hinshaw. 2001. Three-dimensional reconstruction of dynamin in the constricted state. Nat Cell Biol 3:922-926.

37. Ramachandran, R., and S. L. Schmid. 2008. Real-time detection reveals that effectors couple dynamin's GTP-dependent conformational changes to the membrane. The EMBO journal 27:27-37.
38. McMahon, H. T., and I. G. Mills. 2004. COP and clathrin-coated vesicle budding: different pathways, common approaches. Current opinion in cell biology 16:379-391.
39. Devaux, P. F. 2000. Is lipid translocation involved during endo- and exocytosis? Biochimie 82:497-509.
40. Aranda-Espinoza, H., A. Berman, N. Dan, P. Pincus, and S. Safran. 1996. Interaction between inclusions embedded in membranes. Biophysical journal 71:648-656.
41. Chou, T., K. S. Kim, and G. Oster. 2001. Statistical thermodynamics of membrane bending-mediated protein-protein attractions. Biophysical journal 80:1075-1087.
42. Fattal, D. R., and A. Ben-Shaul. 1993. A molecular model for lipid-protein interaction in membranes: the role of hydrophobic mismatch. Biophysical journal 65:1795-1809.
43. Fournier, J. B. 1999. Microscopic membrane elasticity and interactions among membrane inclusions: interplay between the shape, dilation, tilt and tilt-difference modes. European Physical Journal B 11:261-272.
44. Kozlovsky, Y., J. Zimmerberg, and M. M. Kozlov. 2004. Orientation and interaction of oblique cylindrical inclusions embedded in a lipid monolayer: a theoretical model for viral fusion peptides. Biophysical journal 87:999-1012.
45. Landau, L. D., and E. M. Lifshitz. 1986. Theory of elasticity. Pergamon, oxford.
46. Halstenberg, S., T. Heimburg, T. Hianik, U. Kaatze, and R. Krivanek. 1998. Cholesterol-induced variations in the volume and enthalpy fluctuations of lipid bilayers. Biophysical journal 75:264-271.
47. Niggemann, G., M. Kummrow, and W. Helfrich. 1995. The bending rigidity of phosphatidylcholine bilayers. Dependence on experimental methods, sample cell sealing and temperature. J. Phys. II 5:413-425.
48. Evans, E., and D. Needham. 1987. Physical properties of surfactant bilayer membranes: thermal transition,elasticity, rigidity, cohesion, and colloidal interactions. Journal of Physical Chemistry 91:4219-4228.
49. Hamm, M., and M. Kozlov. 1998. Tilt model of inverted amphiphilic mesophases. European Physical Journal B 6:519-528.
50. May, S., Y. Kozlovsky, A. Ben-Shaul, and M. M. Kozlov. 2004. Tilt modulus of a lipid monolayer. Eur Phys J E Soft Matter 14:299-308.
51. Kozlov, M. M., S. Leikin, and R. P. Rand. 1994. Bending, hydration and interstitial energies quantitatively account for the hexagonal-lamellar-hexagonal reentrant phase transition in dioleoylphosphatidylethanolamine. Biophysical journal 67:1603-1611.
52. Kozlov, M. M., and M. Winterhalter. 1991. Elastic moduli and neutral surface for strongly curved monolayers. Analysis of experimental results. J.Phys.II France 1:1085-1100.
53. Leikin, S., M. M. Kozlov, N. L. Fuller, and R. P. Rand. 1996. Measured effects of diacylglycerol on structural and elastic properties of phospholipid membranes. Biophysical journal 71:2623-2632.

54. Fuller, N., and R. P. Rand. 2001. The influence of lysolipids on the spontaneous curvature and bending elasticity of phospholipid membranes. Biophysical journal 81:243-254.
55. Marsh, D. 2007. Lateral pressure profile, spontaneous curvature frustration, and the incorporation and conformation of proteins in membranes. Biophysical journal 93:3884-3899.
56. Illya, G., R. Lipowsky, and J. C. Shillcock. 2005. Effect of chain length and asymmetry on material properties of bilayer membranes. The Journal of chemical physics 122:244901.
57. Chen, Z., and R. P. Rand. 1997. The influence of cholesterol on phospholipid membrane curvature and bending elasticity. Biophysical journal 73:267-276.

Figure legends

Fig. 1. Schematic representation of lipid monolayer bending (lipid molecules shown in light blue) by insertion of a cylindrical inclusion (shown in dark blue), where L is the half distance between the inclusions, h is the monolayer thickness, and r is the inclusion radius. (a) The monolayer is flat before the inclusion insertion; (b) the monolayer bends as a result of inclusion insertion.

Fig. 2. Different cases of monolayer coupling within a bilayer. (a) Laterally uncoupled monolayers. The inclusions (rectangles) are inserted only into a small fragment of a large membrane. The two monolayers of the fragment can independently exchange lipids with the monolayers of the surrounding membrane which plays a role of lipid reservoir (the exchange is indicated by the arrows). (b) Laterally coupled monolayers. The inclusions are inserted across the whole area of a closed membrane. The effects of slow trans-monolayer flip-flop of lipids are neglected.

Fig. 3. Qualitative essence of the mechanism of membrane bending by small cylindrical inclusions. The case of *laterally coupled* monolayers. (a) A shallow inclusion insertion expands the upper layer of the membrane (left). Partial relaxation of the generated stresses results in positive curvature ($J > 0$) (right). (b) Deeper insertion produces an expansion of the upper monolayer (left), which due to the lateral coupling generates stresses in the lower monolayer leading to positive membrane curvature (right). (c) Insertion in the bilayer mid plane generates symmetrically distributed stresses, causing an overall membrane expansion but no curvature. (d) Insertion into the lower monolayer expands the lower part of the membrane, hence generating negative curvature ($J < 0$).

Fig. 4. Qualitative essence of the mechanism of membrane bending by small cylindrical inclusions. The case of *laterally uncoupled* monolayers. (a) A shallow inclusion insertion expands the upper part of the upper monolayer (left), which generates a positive curvature of the upper monolayer leading to positive curvature of the whole membrane ($J > 0$) (right). (b) Deeper insertion produces a bare expansion of the upper monolayer, which, due to the monolayer uncoupling, does not generate curvature. (c) Insertions in the lower portion of the upper monolayer (left) induces negative membrane curvature ($J < 0$).

Fig. 5. A typical conformation of a membrane with cylindrical inclusions (dark blue). (a) The case of laterally uncoupled monolayers (where the second monolayer is not considered to influence the ability to bend). The membrane shape corresponds to the preferred shape of the upper monolayer containing the inclusions as if the lower monolayer (depictured in gray) would not resist bending and just fit the upper one. (b) The case of laterally uncoupled monolayers. The membrane shape is determined by the interplay of the tendency of the upper monolayer to adopt the conformation presented in (a) and the resistance of the lower monolayer to bend. (c) The case of laterally coupled monolayers. The shear strain (dimensionless) in the monolayers is represented as a logarithmic color scale.

Fig. 6. Monolayer spontaneous curvature plotted as a function of the inclusion area fraction for a 0.8 nm depth of insertion.

Fig. 7. Spontaneous curvature for an inclusion plotted as a function of the position of the center of the inclusion for (a) uncoupled, and (b) coupled monolayers. Cartoons of the bilayer are shown for different insertion depths.

Fig. 8. Sensitivity of the effective spontaneous curvature of the inclusion, ς_{inc}, to the monolayer thickness. (a) ς_{inc} as a function of the position of the center of the inclusion for different values of the monolayer thicknesses h , where h can either be 1.8, 2.0 or 2.2nm. (b) ς_{inc} as a function of the monolayer thickness h for the insertion depth of 0.8nm.

Fig. 9. Energetic penalty per unit length of the inclusion plotted as a function of the depth of the insertion for coupled monolayers.

Fig. 10. The range of α-helix area fractions required to form cylindrical membrane tubes of diameter 35-50 nm, plotted as a function of the position of the center of the inclusion, for uncoupled (red) and coupled (gray) monolayers. The maximal possible area fractions of α-helices for endophilin and amphiphysin are represented by straight lines.

Fig. C1. The effective spontaneous curvature of inclusion as a function of the position of the center of the inclusion in the case of coupled monolayers (a) without any lateral stress profile and (b) with a lateral stress profile accounting for a monolayer spontaneous curvature in the initial state $J_s^0 = -0.1nm^{-1}$.

Fig. C2. The energy penalty of the inclusion insertion per inclusion unit length as a function of the position of the center of the inclusion in the case of coupled monolayers (a) without any lateral stress profile and (b) with a lateral stress profile accounting for a monolayer spontaneous curvature in the initial state $J_s^0 = -0.1nm^{-1}$,.

Fig. D1. Sensitivity of the effective spontaneous curvature of the inclusion, ς_{inc}, to the specific value of the transverse shear modulus λ_{xzxz}.

Fig. D2. Sensitivity of the effective spontaneous curvature to (a) the monolayer thickness and (b) the transverse shear modulus for the case of coupled monolayers.

Fig. D3. Sensitivity of the energy penalty of the inclusion insertion per inclusion unit length in the case of coupled monolayers to (a) the monolayer thickness h and (b) the transverse shear modulus λ_{xzxz} .

Fig. D4. Sensitivity of the effective spontaneous curvature to the inclusion radius for the cases of (a) uncoupled monolayers, and (b) coupled monolayers.

Fig. 1

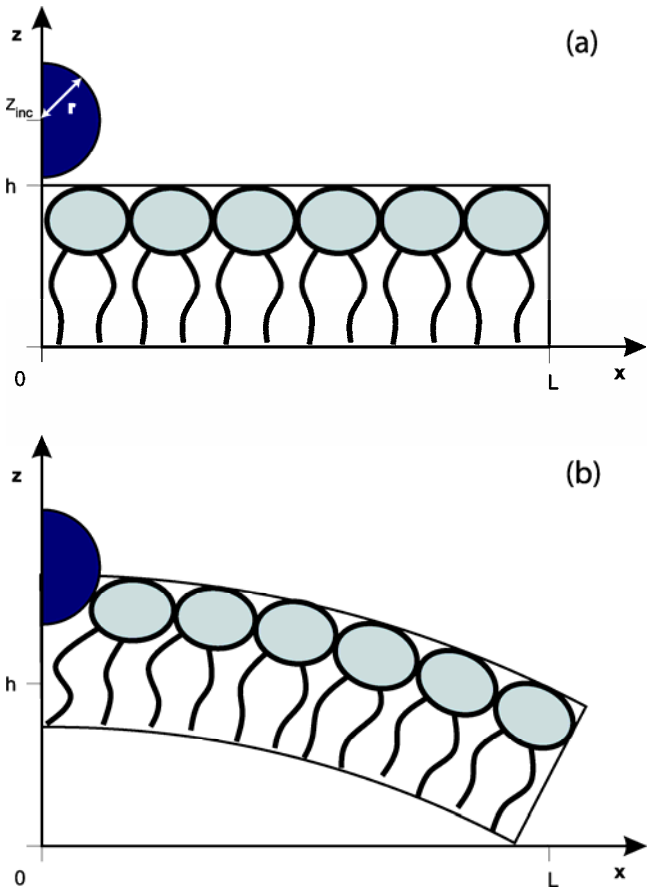

Fig. 2

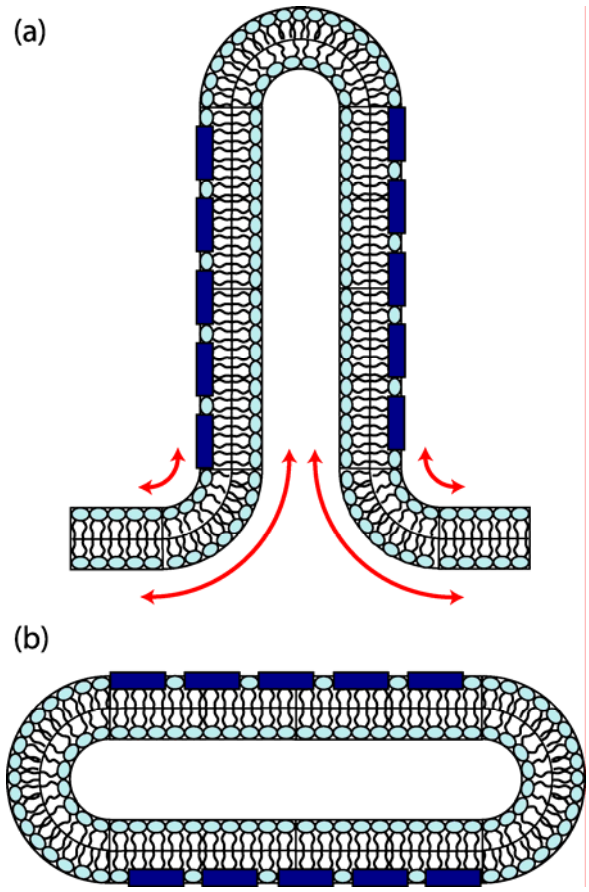

Fig. 3

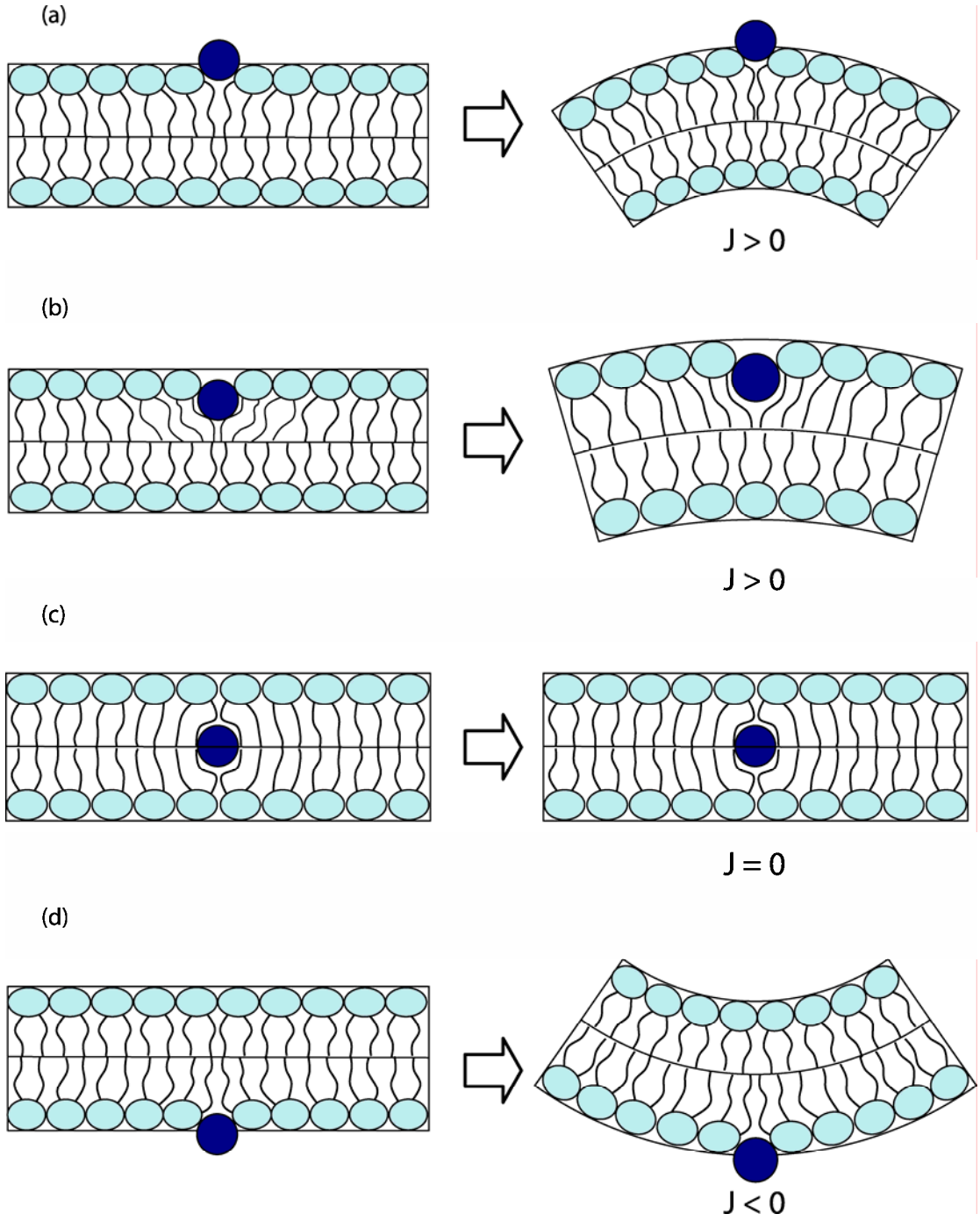

Fig. 4

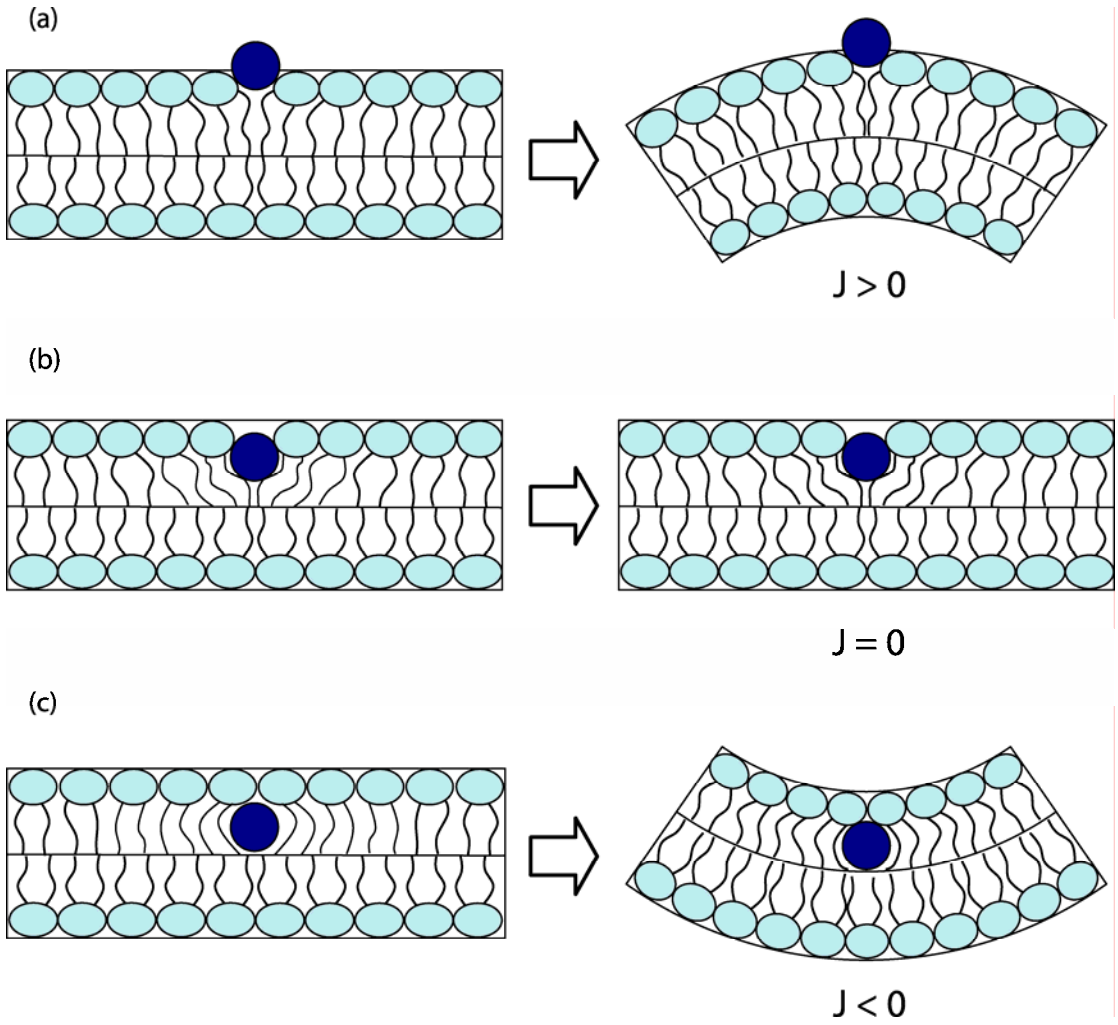

Fig. 5

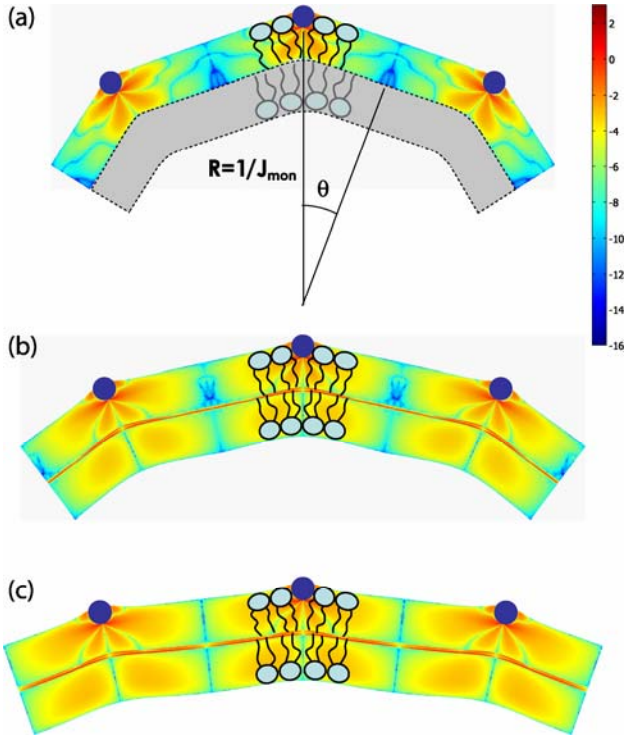

Fig. 6

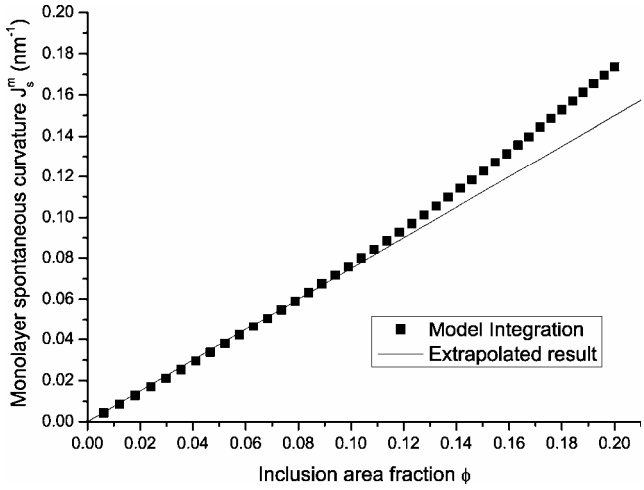
Monolayer spontaneous curvature J_s^m (nm^{-1})
Inclusion area fraction ϕ
Model Integration
Extrapolated result
0.00
0.02
0.04
0.06
0.08
0.10
0.12
0.14
0.16
0.18
0.20

Fig. 7

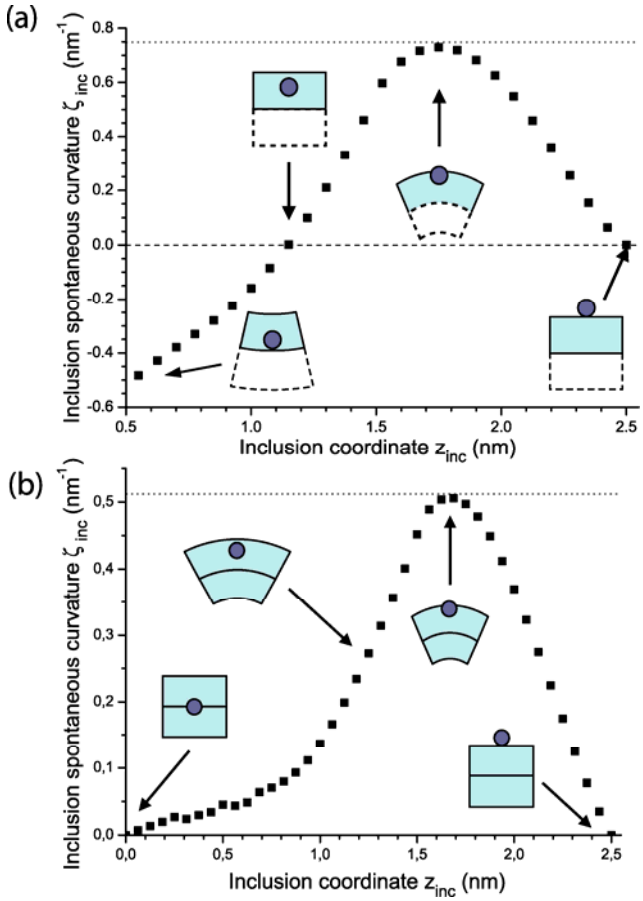
(a)
Inclusion spontaneous curvature ζ_{inc} (nm^{-1})
0.8
0.6
0.4
0.2
0.0
-0.2
-0.4
-0.6
0.5
1.0
1.5
2.0
2.5
Inclusion coordinate z_{inc} (nm)
(b)
Inclusion spontaneous curvature ζ_{inc} (nm^{-1})
0,5
0,4
0,3
0,2
0,1
0,0
0,0
0,5
1,0
1,5
2,0
2,5
Inclusion coordinate z_{inc} (nm)

Fig. 8

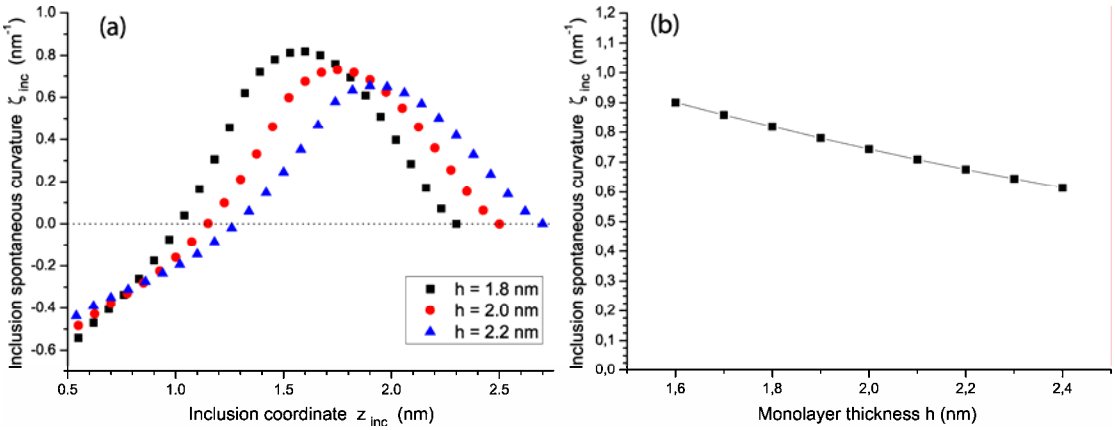
(a)
Inclusion spontaneous curvature ζ_{inc} (nm^{-1})
Inclusion coordinate z_{inc} (nm)
h = 1.8 nm
h = 2.0 nm
h = 2.2 nm
(b)
Inclusion spontaneous curvature ζ_{inc} (nm^{-1})
Monolayer thickness h (nm)

Fig. 9

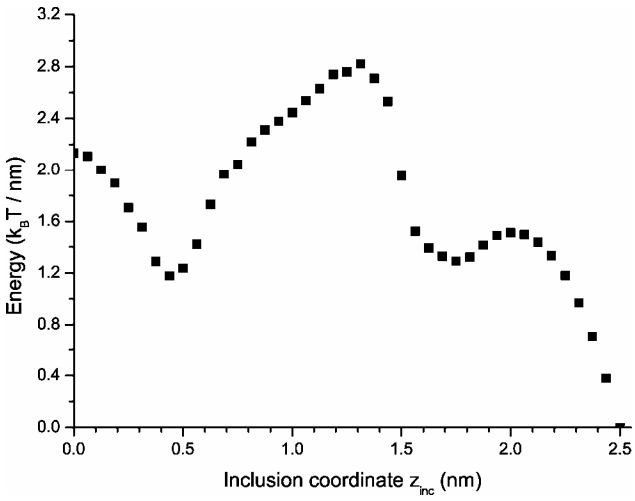
Energy ($k_B T$ / nm)
Inclusion coordinate z_{inc} (nm)
3.2
2.8
2.4
2.0
1.6
1.2
0.8
0.4
0.0
0.0
0.5
1.0
1.5
2.0
2.5

Fig. 10

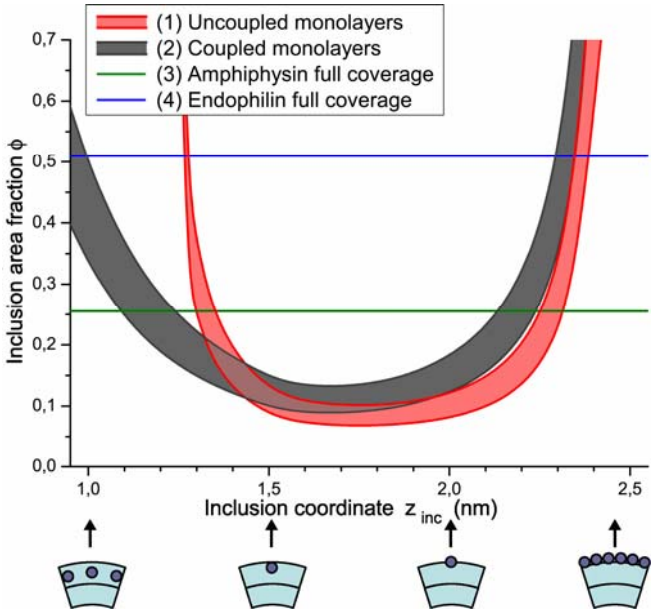
(1) Uncoupled monolayers
(2) Coupled monolayers
(3) Amphiphysin full coverage
(4) Endophilin full coverage
Inclusion area fraction ϕ
0,0
0,1
0,2
0,3
0,4
0,5
0,6
0,7
1,0
1,5
2,0
2,5
Inclusion coordinate z inc (nm)

Fig. C1

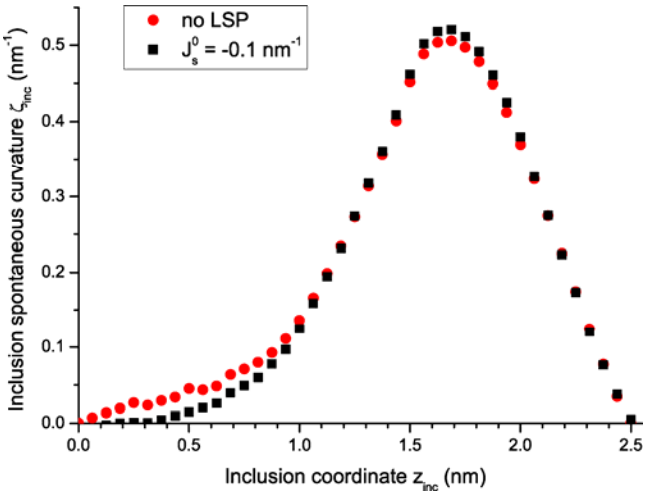
no LSP
J_s^0 = -0.1 nm^{-1}
Inclusion spontaneous curvature ζ_{inc} (nm^{-1})
Inclusion coordinate z_{inc} (nm)
0.0
0.1
0.2
0.3
0.4
0.5
0.0
0.5
1.0
1.5
2.0
2.5

Fig. C2

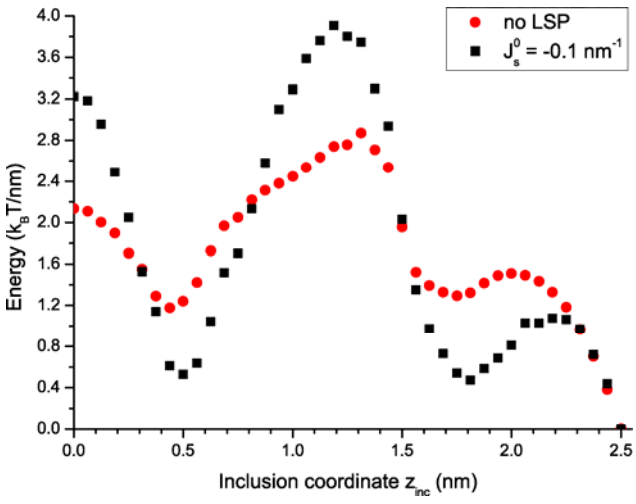
no LSP
J_s^0 = -0.1 nm^{-1}
Energy (k_BT/nm)
Inclusion coordinate z_{inc} (nm)
0.0
0.4
0.8
1.2
1.6
2.0
2.4
2.8
3.2
3.6
4.0
0.0
0.5
1.0
1.5
2.0
2.5

Fig. D1

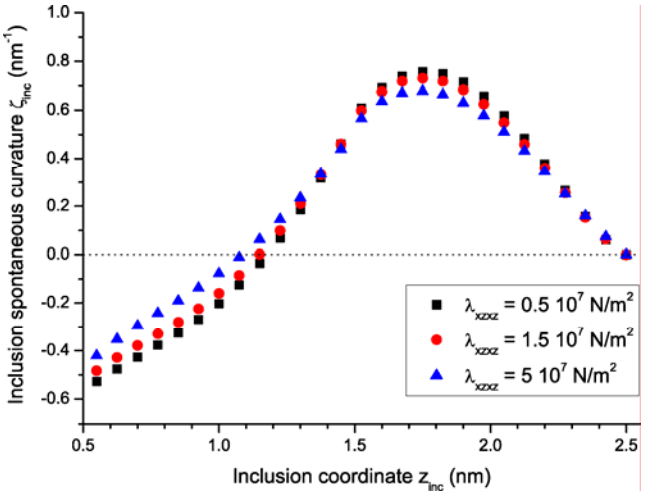
Inclusion spontaneous curvature ζ_{inc} (nm^{-1})
Inclusion coordinate z_{inc} (nm)
λ_{xzxz} = 0.5 10^7 N/m^2
λ_{xzxz} = 1.5 10^7 N/m^2
λ_{xzxz} = 5 10^7 N/m^2

Fig. D2

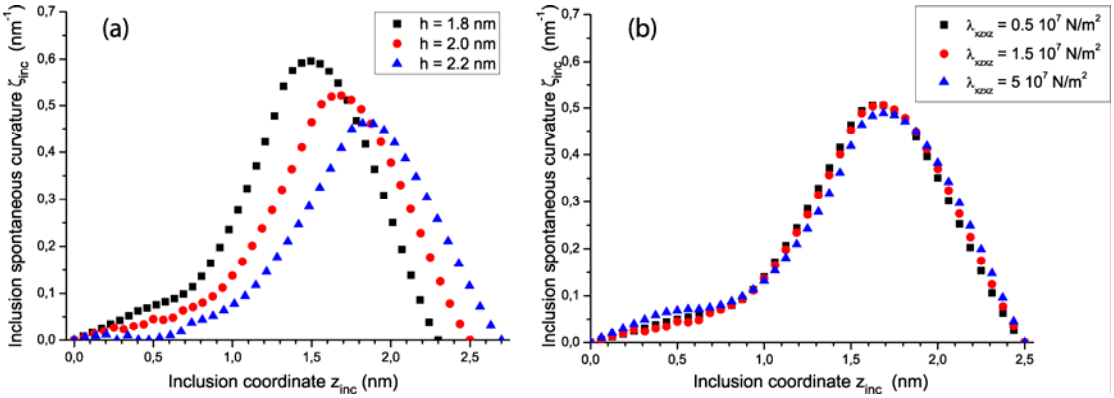
(a)
h = 1.8 nm
h = 2.0 nm
h = 2.2 nm
Inclusion spontaneous curvature ζ_{inc} (nm^{-1})
Inclusion coordinate z_{inc} (nm)
(b)
λ_{szxz} = 0.5 10^7 N/m^2
λ_{szxz} = 1.5 10^7 N/m^2
λ_{szxz} = 5 10^7 N/m^2
Inclusion spontaneous curvature ζ_{inc} (nm^{-1})
Inclusion coordinate z_{inc} (nm)

Fig. D3

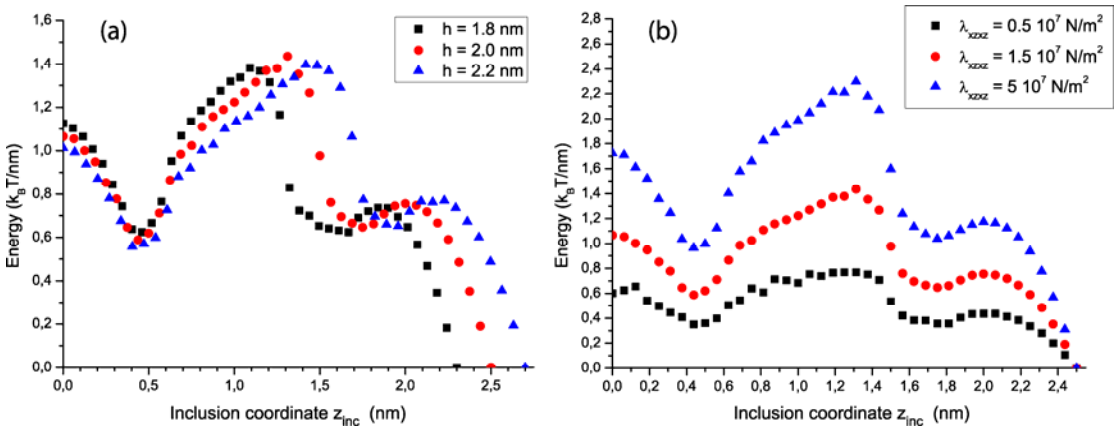
(a)
h = 1.8 nm
h = 2.0 nm
h = 2.2 nm
Energy (k_BT/nm)
Inclusion coordinate z_{inc} (nm)
(b)
λ_{xzxz} = 0.5 10^7 N/m^2
λ_{xzxz} = 1.5 10^7 N/m^2
λ_{xzxz} = 5 10^7 N/m^2
Energy (k_BT/nm)
Inclusion coordinate z_{inc} (nm)

Fig. D4

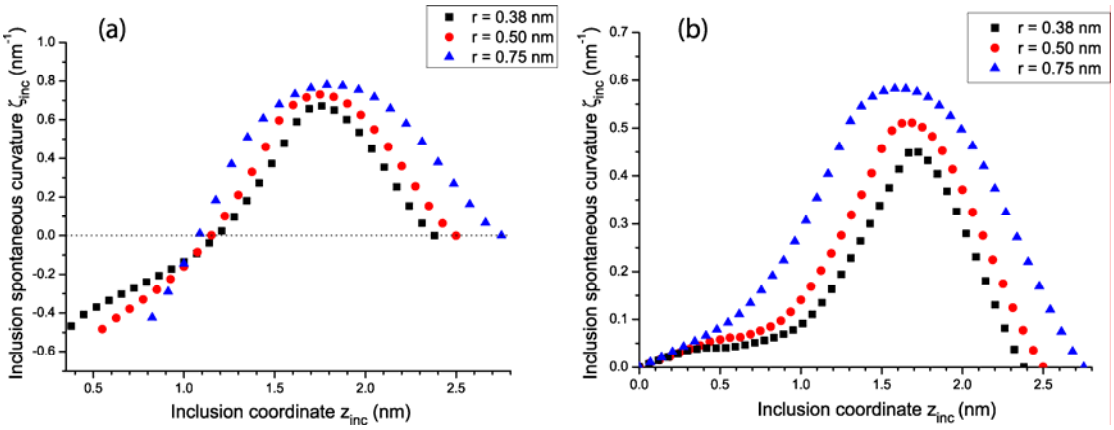
(a)
r = 0.38 nm
r = 0.50 nm
r = 0.75 nm
Inclusion spontaneous curvature r_{inc} (nm^{-1})
Inclusion coordinate z_{inc} (nm)
(b)
r = 0.38 nm
r = 0.50 nm
r = 0.75 nm
Inclusion spontaneous curvature r_{inc} (nm^{-1})
Inclusion coordinate z_{inc} (nm)